University of Louisville

ThinkIR: The University of Louisville's Institutional Repository

Substellar and low-mass dwarf identification with near-infrared imaging space observatories

Benne W. Holwerda
University of Louisville, benne.holwerda@louisville.edu

J. S. Bridge
University of Louisville

R. Ryan
STScI

M. A. Kenworthy
Leiden Observatory Research Institute

N. Pirzkal
STScI

See next page for additional authors

Follow this and additional works at: https://ir.library.louisville.edu/faculty

Part of the Astrophysics and Astronomy Commons

ThinkIR Citation

Authors

Benne W. Holwerda, J. S. Bridge, R. Ryan, M. A. Kenworthy, N. Pirzkal, M. Andersen, S. Wilkins, R. Smit, S. R. Bernard, T. Meshkat, R. Steele, and R. C. Bouwens

Substellar and low-mass dwarf identification with near-infrared imaging space observatories[*]

B. W. Holwerda[1,2], J. S. Bridge[1], R. Ryan[3], M. A. Kenworthy[2], N. Pirzkal[3], M. Andersen[4], S. Wilkins[5], R. Smit[6], S. R. Bernard[7,8], T. Meshkat[9], R. Steele[1], and R. C. Bouwens[2]

[1] Department of Physics and Astronomy, 102 Natural Science Building, University of Louisville, Louisville, KY 40292, USA
e-mail: benne.holwerda@louisville.edu
[2] Leiden Observatory, University of Leiden, Niels Bohrweg 2, 2333 CA, Leiden, The Netherlands
[3] Space Telescope Science Institute, 3700 San Martin Drive, Baltimore, MD 21218, USA
[4] Gemini Observatory, Southern Operations Center, c/o AURA, Casilla 603, La Serena, Chile
[5] Department of Physics and Astronomy, University of Sussex, Brighton, BN1 9QH, Sussex, UK
[6] Kavli Institute of Cosmology, c/o Institute of Astronomy, Madingley Road, Cambridge CB3 0HA, UK
[7] School of Physics, The University of Melbourne, VIC 3010, Australia
[8] ARC Centre of Excellence for All-sky Astrophysics (CAASTRO), Australia
[9] IPAC, California Institute of Technology, Pasadena, CA 91125, USA

ABSTRACT

Aims. We aim to evaluate the near-infrared colors of brown dwarfs as observed with four major infrared imaging space observatories: the *Hubble* Space Telescope (HST), the *James Webb* Space Telescope (JWST), the *Euclid* mission, and the WFIRST telescope.
Methods. We used the SPLAT SPEX/ISPEX spectroscopic library to map out the colors of the M-, L-, and T-type dwarfs. We have identified which color–color combination is optimal for identifying broad type and which single color is optimal to then identify the subtype (e.g., T0-9). We evaluated each observatory separately as well as the narrow-field (HST and JWST) and wide-field (*Euclid* and WFIRST) combinations.
Results. The *Euclid* filters perform equally well as HST wide filters in discriminating between broad types of brown dwarfs. WFIRST performs similarly well, despite a wider selection of filters. However, subtyping with any combination of *Euclid* and WFIRST observations remains uncertain due to the lack of medium, or narrow-band filters. We argue that a medium band added to the WFIRST filter selection would greatly improve its ability to preselect brown dwarfs its imaging surveys.
Conclusions. The HST filters used in high-redshift searches are close to optimal to identify broad stellar type. However, the addition of F127M to the commonly used broad filter sets would allow for unambiguous subtyping. An improvement over HST is one of two broad and medium filter combinations on JWST: pairing F140M with either F150W or F162M discriminates very well between subtypes.

Key words. Galaxy: disk – Galaxy: halo – Galaxy: stellar content – gamma rays: stars – brown dwarfs

1. Introduction

Several near-infrared space telescope missions are planned in the coming decade; the *James Webb* Space Telescope (JWST) the *Euclid* mission, and the Wide-field Infrared Survey Telescope (WFIRST). Together with the Wide Field Camera 3 (WFC3) on board the *Hubble* Space Telescope (HST), they represent an opportunity to study the structure of the Milky Way through the distribution of red and brown dwarf stars (M-, L-, T-, and Y-type; Kirkpatrick 2005; Burgasser et al. 2006; Cruz et al. 2007; Kirkpatrick et al. 2011; Dieterich et al. 2014; Tinney et al. 2014). All of these observatories will survey extragalactic fields that will overlap with observations of the disk and halo components of the Milky Way that include these stellar and substellar objects.

In this respect, the HST/WFC3 observations of extragalactic fields (e.g., CANDELS and BoRG; Grogin et al. 2011; Koekemoer et al. 2011; Trenti et al. 2011) are a guide into how one could use the stars found in extragalactic fields to map our

own Milky Way. This by-product of the extragalactic surveys has been explored already, often combining near-infrared images with grism spectra or proper motion data to positively identify brown dwarfs.

For example, Pirzkal et al. (2005) found M-type brown dwarfs in the *Hubble* Ultra Deep Field (HUDF; Beckwith et al. 2006), and Ryan et al. (2005) identified L- and T-type dwarfs in a small set of Advanced Camera for Surveys (ACS) parallel observations. These studies primarily measure the scale height of the Milky Way disk.

Pirzkal et al. (2009) mapped M-type dwarfs in the Great Observatories Origins Deep Survey fields (GOODS; Giavalisco et al. 2004) using the grism observations from PEARS (Probing Evolution And Reionization Spectroscopically; Straughn et al. 2009) for positive identification. Similarly, Ryan et al. (2011) and Holwerda et al. (2014) find T-type and M-/L-type dwarfs, respectively, in pure-parallel[1] WFC3 observations. With the increasing

---

[1] A special mode of imaging observations offered on HST: while the main observation is performed with the COS spectrograph, the WFC3 or ACS camera takes undithered imaging. Image quality and exposure time are consequently more limited than targeted observations.

number of sight-lines, primarily a result of the pure-parallel campaigns of the Brightest of Reionizing Galaxies (BoRG; Trenti et al. 2011; Calvi et al. 2016; Bernard et al. 2016), statistics have improved to a point where one can model more than just the scale height of the Galactic thin disk of the Galaxy. One can model simultaneously the thickness of the disk and the the stellar halo (van Vledder et al. 2016). A second goal of these studies is to accurately map the scale height as a function of substellar dwarf subtype. Scale height as a function of subtype links the relation between Galactic wide star-formation history, the dynamical heating of the substellar population, and the cooling of the substellar dwarfs over time (Ryan et al. 2017). They predict a thicker Galactic disk for later subtypes with the slope of the increase primarily depending on the Galactic star-formation history.

A substantial motivation for these studies is to exclude Galactic brown dwarfs from the selections of high-redshift objects, which they resemble in near-infrared color space (Caballero et al. 2008; Wilkins et al. 2014; Holwerda et al., in prep.) and in direct imaging surveys in search of extrasolar planets. Because brown dwarfs have been found in observations that were not specifically designed for their discovery, we explore the filter sets on current and future near-infrared observatories to identify which combination of filters is optimal to identify brown dwarfs and their (sub)types.

It is reasonable to expect that of the multitude of red or brown dwarfs still to be discovered, a great many will be found in high Galactic latitude surveys designed to observe the high redshift Universe. Previous work on these objects relied on all-sky surveys (e.g., ALLWISE and 2MASS) with (for extragalactic searches) shallow limits. A much larger volume will be probed by the deep extra-planar extragalactic surveys planned for *Euclid* and WFIRST.

Our aim is to predict which survey will produce the best brown dwarf samples and to make filter choice recommendations for surveys to improve brown dwarf identification. Our approach is largely led by our experiences with the BoRG survey (Ryan et al. 2011; Holwerda et al. 2014) where morphologically identified stars (fully unresolved), a near-infrared color–color selection identified broad brown dwarf types, and a different single color was used to subtype a selection of these brown dwarfs. Our overall assumption in the following is that grism or spectroscopic observations of these brown dwarfs is considered an undesirable or impractical outcome by the high redshift survey teams and that this information is therefore not available, or alternatively, the imaging mode is secondary (parallel observations), making grism observations impractical (e.g., WFIRST guiding for coronagraphic or integral field unit observations).

An astrophysical caveat for this paper is that we assume that all the red and brown dwarfs observed are single stars, even though it is well established that anywhere from 0 to 50% of all these stars are actually in binaries, depending on type and environment (e.g., Joergens et al. 2003; Burgasser & McElwain 2006; Ahmic et al. 2007; Dupuy & Liu 2012; Ward-Duong et al. 2015; Opitz et al. 2016; Shan et al. 2017, and references therein). Most of the later brown dwarfs (L and T) have unique spectral signatures (Burgasser et al. 2016, 2017; Theissen et al. 2018; Bardalez Gagliuffi et al. 2018), causing their colors (especially medium or narrow filters) to be unique. How exactly these change as such stars are in close binaries depends on the mix of stellar types but the range of all SPLAT sources in comparison to just the standard star relations should give some indication. This assumption of no binaries has been made in all the photometric searches for red and brown dwarf stars thus far because simple photometric typing cannot distinguish well

enough between close binaries of different types and single red or brown dwarfs. One can overcome this problem by using methods such as Markov Chain Monte Carlo techniques (MCMC; see van Vledder et al. 2016), which allow for a fraction of the data to be erroneous.

We divide the current and future surveys into narrow-field (HST and JWST) and wide-field (WFIRST and *Euclid*), and combine missions and instruments to search for observations that would be ideal to identify brown dwarfs throughout the disk and halo of our Milky Way. Our goal for this paper is to evaluate filter combinations to separate out broad brown dwarf types (M, L, and T) and colors to subtype each brown dwarf type (e.g., M0-M9 or T0-T5). Our concern here is to explore what will constitute the minimum filter combination to type brown dwarfs reliably. This paper is organized as follows: Sect. 2 summarizes the SPLAT library used to evaluate the filters, Sect. 3 summarizes the observatories we consider here, Sect. 4 presents the results of broadly categorizing brown dwarfs in color–color space, and Sect. 5 discusses how well any single color could be used to subtype those objects identified as bona-fide brown dwarfs. We discuss the results in Sect. 6 with our concluding remarks in Sect. 7.

2. Red and brown dwarf spectra

To map the near-infrared colors of brown dwarfs, we use the PYTHON module SPLAT[2] (Burgasser & SPLAT Development Team 2017). This module contains an online repository of 1701 low-resolution, near-infrared spectra of low-temperature stars and brown dwarfs. It is built on common python packages such as ASTROPY, MATPLOTLIB, NUMPY, PANDAS and SCIPY. We introduced the HST, JWST, WFIRST, and *Euclid* filters into this package using the built-in "custom" filter option for spectrophotometry. All colors reported are derived from Vega magnitudes. Two example tables are shown in Tables A.1 and A.2 for all the standard stars (defining the type) in the various HST filters. Full tables for all four observatories are available at the CDS with this publication.

We use the ensemble of spectra to map out the spectrophotometry using the built-in modules to compute the colors of near-infrared filter combinations. The built-in standard star library (Fig. 1) as well as the full spectral library are both used in the following work. The spectral library and classifications come from Reid et al. (2001), Testi et al. (2001), Allers et al. (2007), and Burgasser (2007).

These spectra may not be representative of the more distant red or brown dwarf stars in the halo or thick disk ; higher surface gravity, lower metallicity, and changes in the NIR absorption features as the C, N, O abundances change.

We used the standard stars from Burgasser et al. (2006), Kirkpatrick et al. (2010), and Cushing et al. (2011) to explore the "ideal" color or color–color track. Using the full SPLAT database, we illustrate the noise and variance that can be expected from a population of brown dwarfs. Red and brown dwarf types are assigned a numerical type with the convention 0-1 (M-types), 1-2 (L-types), 2-3 (T-types) and 3 and above (Y-types), with decimal values denoting the subtype.

3. Observatories

We evaluate the near-infrared filter sets of four space-borne observatories: HST and JWST are pointed, narrow-field observatories, while *Euclid* and WFIRST are wide-field observatories.
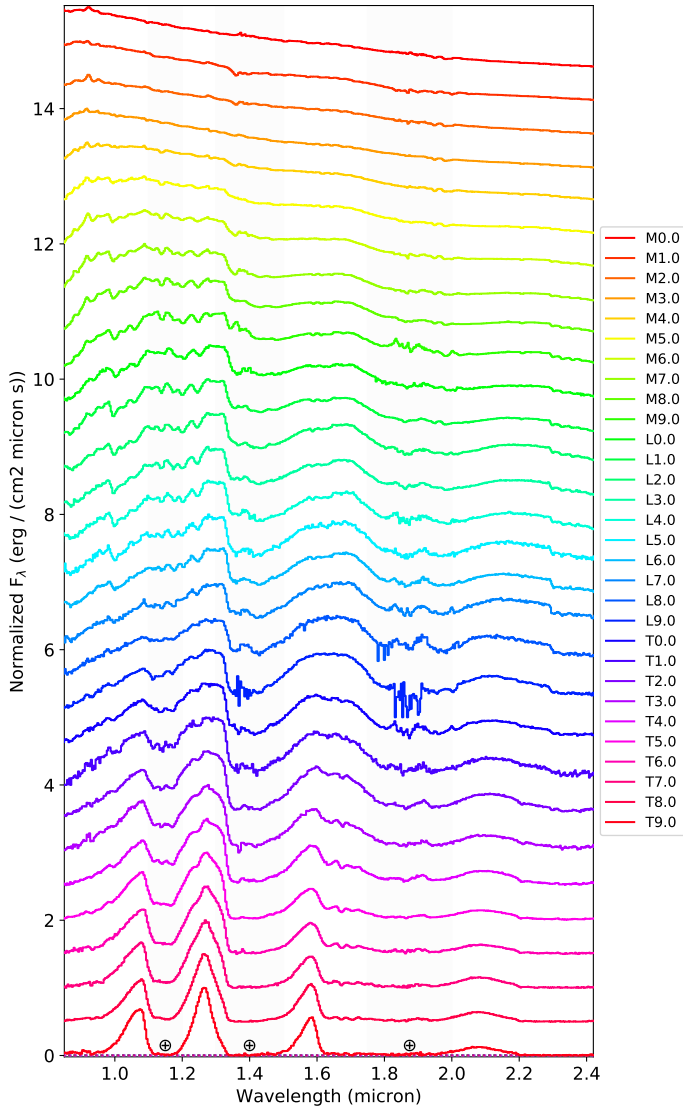
---

[2] http://pono.ucsd.edu/~adam/browndwarfs/splat/

3.1. Hubble Space Telescope Wide Field Camera 3

The Wide Field Camera 3 (WFC3; Kimble et al. 2008) added unique ultraviolet and near-infrared capabilities to the HST when it was installed. We consider the typical set of filters on WFC3 that are used for extragalactic observations: F098M, F105W, F125W, F140M, and F160W. We also include the near-infrared/optical filter F814W in this selection as it is typically available in high-redshift surveys such as CANDELS (Grogin et al. 2011; Koekemoer et al. 2011).

3.2. Hubble Space Telescope Wide Field Camera 3 medium- and narrow-band filters

In addition to the medium and wide filters commonly used in extragalactic surveys, there are some medium- and narrow-band filters to consider. These are mostly within the F125W and F140W wide-band filters: F126N, F127M, F128N, F130N, F132N, F139M, and F153M. Some of these will be centered on the broad absorption features in red or brown dwarf spectra. A similar approach using a wide and a narrow filter has worked well to determine the low-mass end of the stellar initial mass function in Galactic star-formation regions (Najita et al. 2000; Andersen et al. 2006; Da Rio et al. 2012). Narrow-band imaging filters (e.g., J1 or J2 medium-band filters) centered on the methane bands can well be used to type the lower-mass dwarfs (Tinney et al. 2012).

3.3. James Webb Space Telescope

The NIRCam instrument on board the JWST is a versatile instrument with a range of broad, medium- and narrow-band filters. We evaluate the NIRCam F070W, F090W, F115W, F140M, F150W, F150W2, F162M, and F200W filters (Fig. 2). NIRCam also has longer wavelength filters, but we cannot evaluate those filters because of a lack of coverage by the spectra in SPLAT. In Holwerda et al. (in prep.), we found that Spitzer [3.6]–[4.5] μm color correlates well with spectral type for the cooler (>L5) brown dwarfs (see also Kirkpatrick et al. 2011; Pecaut & Mamajek 2013; Skrzypek et al. 2016). It is therefore possible that the longer wavelength filters on NIRCam and the MIRI instrument hold possibilities for improved brown dwarf characterization.

3.4. Euclid

The European Space Agency *Euclid* mission has three main goals: it will be used as a gravitational lensing experiment, a photometric redshift experiment to map baryon acoustic oscillations, and a supernovae search (Laureijs et al. 2011). The design calls for only three filters (*Y*, *J*, and *H*; Fig. 2) in the near-infrared, and a very wide-band filter in the optical (for the gravitational lensing measurements).

For the purposes of this work, the gain from this observatory is that it will scan the entire sky to a depth of $m_J = 24$ and the ecliptic poles to a depth of $m_J = 26$, making *Euclid* photometry universally available in combination with any other observatory's filters. The NIR filters for *Euclid* are wide Y, J and H filters modeled with a simple wavelength window. The PSF is 0.2″ in the NIR filters.

3.5. WFIRST

WFIRST (Dressler et al. 2012; Spergel et al. 2013; Thompson et al. 2013) is NASA's next flagship astrophysical mission. It will have a limited selection of broad near-infrared filters:

Fig. 1. Spectra of the standard stars in SPLAT, defining each sub-type of brown dwarf from M0 to T9 for the 0.9–2.4 μm wavelength range. SPLAT contains spectral standards for dwarf classes M0 through T9, drawn from Burgasser et al. (2006); Kirkpatrick et al. (2010), and Cushing et al. (2011). Near-infrared colors are strongly influenced by the strength of the absorption features at 1.2 μm (methane) and 1.4 μm (water), especially in the later brown dwarf types (T and later).

Therefore, we also evaluate the filter combinations between the first two and latter two observatories. The near-infrared filters of all four observatories are summarized in Fig. 2. The WFIRST and *Euclid* filters are based on mission specifications and measured prototype filters, while the HST and JWST filter transmission curves are measured from flight hardware. We divide the HST medium- and narrow-band filters in two categories, depending on whether or not they are commonly used in extragalactic surveys. One group contains mostly broad filters and the F105M filter that are used for extragalactic surveys, and other encompasses the remaining medium- and narrow-band filters. All four observatories have comparable point spread function (PSF) sizes across this wavelength regime (*FWHM* ~ 0.1 arcsec) so for our purposes, we can assume that to first order, all four observatories will perform equally well in distinguishing stars from galaxies in the near-infrared imaging. The problem is therefore reduced to how well stellar objects can be typed by one or more near-infrared colors.
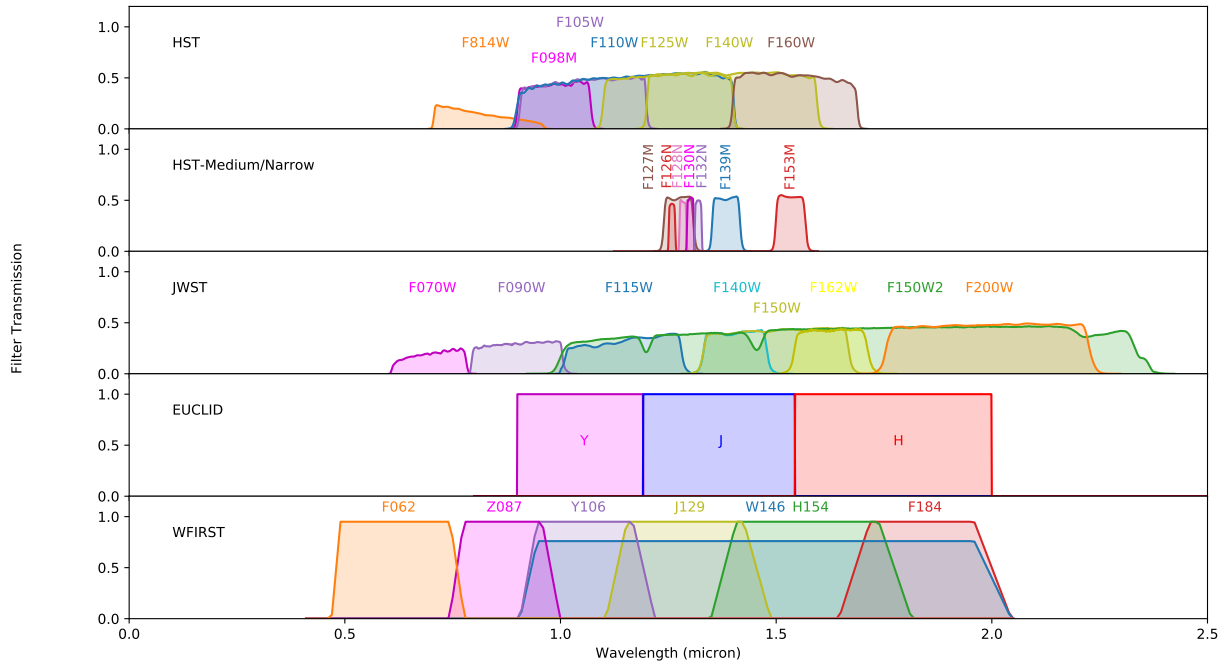
Fig. 2. Overview of all the near-infrared filters in the 0.5–2 *μ*m range for the four space observatories. *Top panel*: typical filters available in high-redshift surveys with *Hubble*. *Second panel*: medium- and narrow-bands available in HST/WFC3 but not generally used in extragalactic surveys. *Third panel*: JWST/NIRCam filter sets available. *Fourth panel*: specified NIR filter requirements for the *Euclid* mission camera. *Fifth panel*: current WFIRST filter set considered for the mission.

F184, H158, J129, W146, Y106, Z087, and F062 for the Wide Field Instrument (Fig. 2). The WFI provides an imaging mode covering 0.76–2.0 *μ*m and a spectroscopy mode covering 1.35–1.95 *μ*m. The wide field focal plane covers an effective field of view of 0.281 deg^2 with a 0.11″ pixel scale and 0.2″ PSF width.

3.6. Morphological identification of stars

All four observatories sample the width of their PSF by approximately two pixels. Our experience with HST suggests that this is enough for a reliable morphological identification of stars ~1.5 magnitudes above the photometric limit of a given survey using the effective radius determined from a growth curve (the ranked list of pixels in each object; see Ryan et al. 2011; Holwerda et al. 2014). Better sampling improves the spread in effective radius for stars into a tighter relation with luminosity. However, the limiting magnitude for differentiating between stars and galaxies is only extended by ~0.2 magnitude. Given that our target is the substellar population of Milky Way dwarfs, the morphological selection is close to identical for different instruments.

3.7. Grism surveys

The scope of this paper is limited to imaging surveys. Specifically, we evaluate whether or not the combination of existing and planned surveys can readily identify red or brown dwarf populations, or how a small filter addition can convert such surveys into an optimal dwarf census. However, these four observatories all have grism low-resolution spectroscopy capabilities.

HST/WFC3 and ACS grism observations have already been used to identify brown/red dwarf stars in our Galaxy; Pirzkal et al. (2005, 2009) reported M-dwarfs in ACS grism data, and Masters et al. (2012) reported the discovery of three late >T4.5-type dwarfs in the WFC3 Infrared Spectroscopic Parallels (WISP) survey. Similarly, one can expect more substellar objects

to be subtyped in the 3D-HST (Brammer et al. 2012; Skelton et al. 2014; Momcheva et al. 2016) and FIGS (Tilvi et al. 2016; Pirzkal et al. 2017) WFC3 grism surveys. The limiting magnitude on shallow grism observations is effectively $m_J = 23$ (Masters et al. 2012) and well over two magnitudes deeper in similar time investment in pure-parallel imaging observations (Ryan et al. 2011; Holwerda et al. 2014).

WFIRST will observe ~2000 deg^2 with its grism element to depths of $m_{AB} \sim 26$ with a wavelength range of 1.35–1.89 *μ*m (Spergel et al. 2013, 2015). In effect this will be an ideal brown/red dwarf dataset, covering at least one of the wide absorption features that define the later brown dwarf types (Fig. 1).

In this paper, we do not consider these grism observations only as matter of strategy and a way to limit the scope of the work. Our considerations for not including grism comparisons are the following: (1) imaging observations are easier to compare across instruments for their efficiency at typing red or brown dwarfs, (2) the aim of the paper is to ascertain whether certain extragalactic programs can be used for red or brown dwarf typing as is or require an amended observing strategy, and (3) the possible use of future pure-parallel observations similar to BoRG (by HST, JWST or WFIRST) in the typing of brown/red dwarfs and the scale of the Milky Way.

3.8. Proper motion identification

Many of the red and brown dwarfs in the solar neighborhood have been identified using their proper motion (Kirkpatrick et al. 2014, 2016; Robert et al. 2016; Kuchner et al. 2017). In the case of the higher latitude imaging surveys, this may still be possible but it will be proportionally more difficult because proper motions for these more distant, fainter objects are expected to be on the order of milliarcseconds, especially in the case of halo objects. Ryan et al. (2005) used proper motion to help identify
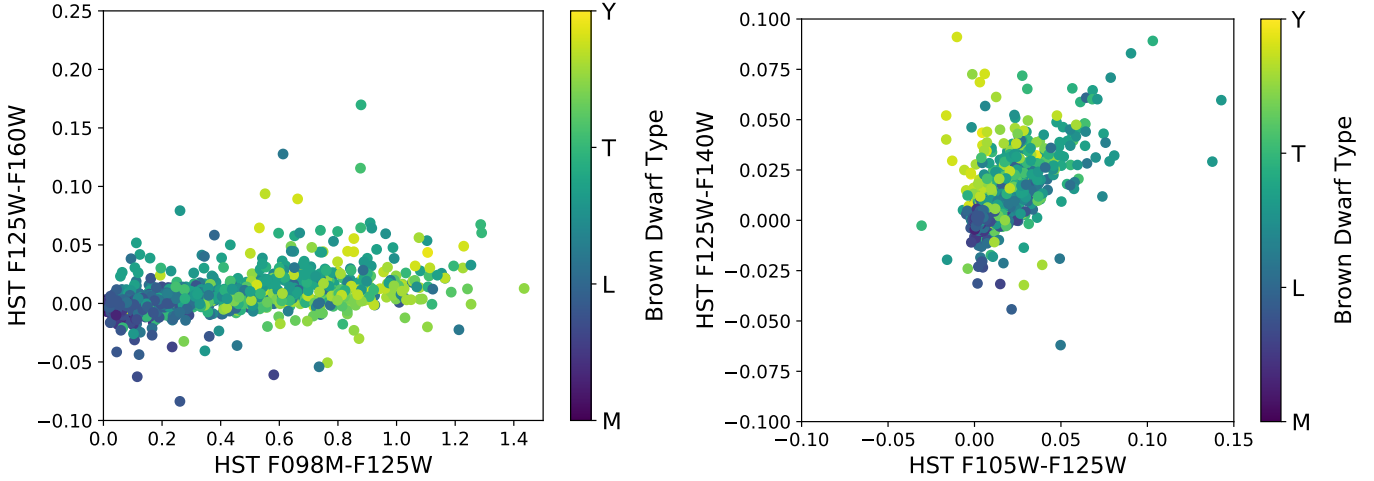
Fig. 3. HST color–color combinations for brown dwarf selection as a class of objects. These are is the common filter combinations for HST pure-parallel observations (Ryan et al. 2011; Holwerda et al. 2014; van Vledder et al. 2016).

M-type dwarfs and this could be a viable verification method, depending on the observing strategy of the extragalactic surveys (ideally multiple, well-spaced epochs). In reality, cadence and PSF-centering are dictated by spacecraft limits and searches for extragalactic transients (e.g., supernovae), and they may be well-suited for proper motion studies.

Imaging surveys are more efficient at covering larger areas to a greater depth and with multiple pointings than grism surveys, although they sacrifice some accuracy in dwarf typing in the process. To map the structure of the Galaxy in dwarf stars, multiple lines-of-sight and a large volume will be necessary.

4. Brown dwarf selection

Ryan et al. (2011) and Holwerda et al. (2014) used two near-infrared colors observed with WFC3 to identify objects as dwarf stars, separating them from high-redshift objects. Subsequently, these near-infrared colors can be used to identify the broad brown dwarf types. By necessity, these were the F098M, F125W and F160W of the BoRG survey (Trenti et al. 2011). Stellar objects that were already morphologically identified were typed further as M-type dwarfs, and then subtyped using an optical-near-infrared color. Here, we first evaluate different two color filter combinations to separate out broad dwarf star type. To evaluate the resolving power of a single color mapping to red or brown type, we use the Spearmann ranking (ρ). If type increases or decreases monotonically with color, the Spearmann ranking is close to unity (± 1), representing an ideal case to use that color for subtyping.

Table A.3 shows the Spearman ranking between the brown dwarf type and HST color pairs. The best combinations are $Y_{F105W} - J_{F125W}$ combined with $J_{F125W} - JH_{F140M}$, when only considering broad filters, often employed for extra-galactic work. This is remarkably close to the BoRG[z9] filter combinations (Calvi et al. 2016; Bernard et al. 2016) but differs from the $Y_{F098M} - J_{F125W}/J_{F125W} - H_{F160W}$ filter combinations used earlier in *Hubble* pure-parallel observations (Holwerda et al. 2014; van Vledder et al. 2016). The difference in Spearman ranking between these two filter combinations is only moderate (Table A.3); both combinations perform similarly in distinguishing broad types.

Figure 3 shows the optimal HST filter combinations identified by the Spearman ranking for separating out dwarf types as
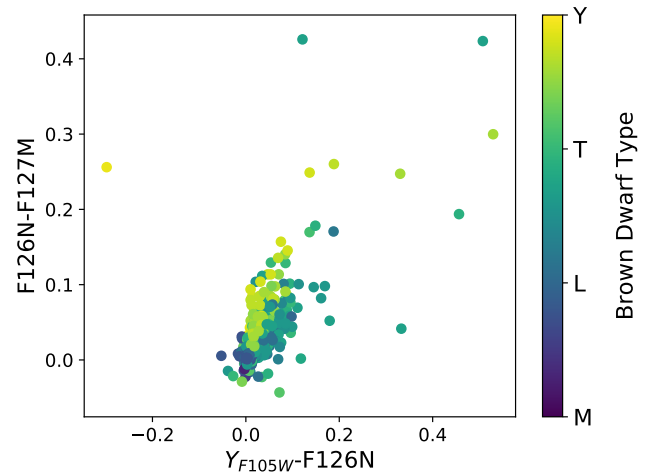

Fig. 4. Optimal HST color–color selection including medium- and narrow-band filters not often used in extragalactic surveys. Separation into broad categories is not dissimilar to the performance of the broad-band filters already in use.

well as the color-color combination used most often so far, i.e. based on existing data. Both discriminate the broad brown dwarf populations reasonably well. Ongoing searches for brown dwarfs in BoRG WFC3 fields will be able to reliably type the brown dwarfs using either filter combination.

We can expand the color possibilities if we include the medium- and narrow-band filters that are not typically used in extragalactic surveys. The two-color selection improves somewhat when one medium filter often used in extragalactic surveys (F105W) is combined with two filters not commonly used in extragalactic filters (F126N, F127M; Fig. 4). Separation of the dwarf broad types is somewhat better with this filter combination than the extragalactic filter combinations (Figs. 3 and 4). We note, however, that once this is applied to the full SPLAT sample of red or brown dwarfs, the relation is not as clear cut.

The many filters available on JWST offer the opportunity to discriminate among brown dwarf types and subtypes, as they span the deep absorption features in the later types. The best combination to discern between brown dwarf types is $F140M - F150W$ and $F150W - F162M$ (Fig. 5). This filter combination cleanly separates the different dwarf subtypes with a clear
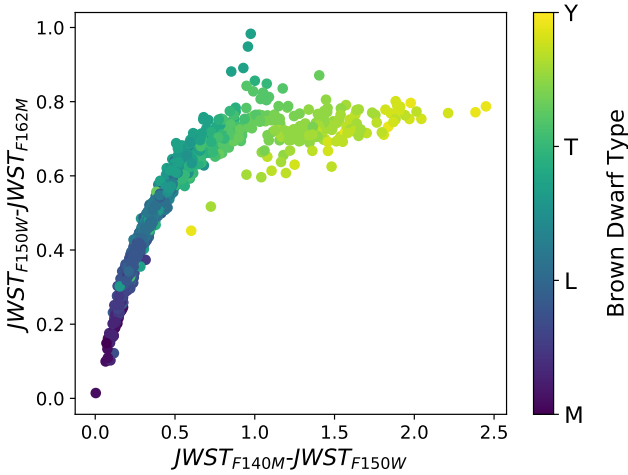
Fig. 5. Relation between JWST F140W, F150W, and F162M colors and the brown dwarf type and subtype for all the objects in the SPLAT catalog. The combined broad/medium filter set separates out the type and subtype very well for all, outperforming the HST F125W/F127M filter combination.
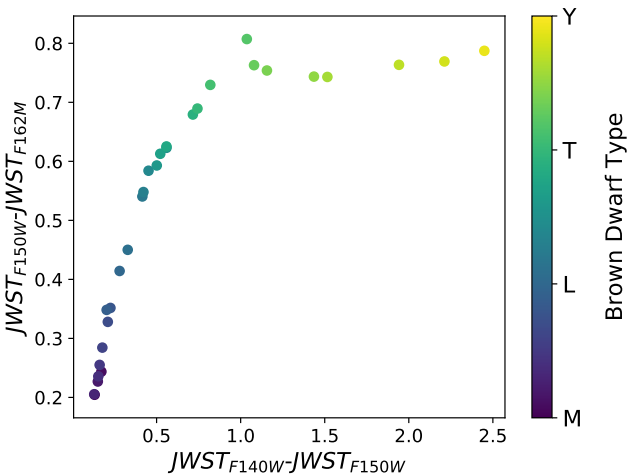

Fig. 6. JWST color–color selections for brown dwarf standard stars.

Fig. 7. *Euclid* color–color plot of all the brown dwarfs in SPLAT. The broad filters of *Euclid* identify brown dwarfs as a population, but do not discriminate between broad classes.
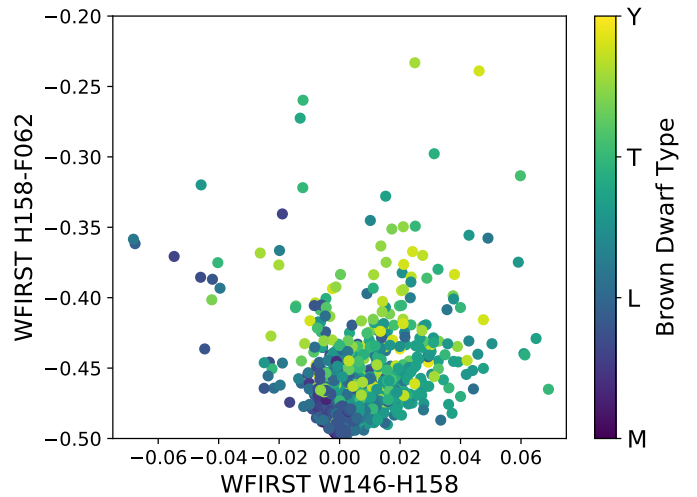
Fig. 8. WFIRST color–color plot of all the brown dwarfs in SPLAT. The W146, H158 and F062 filters separate out the broad brown dwarf types –M, L, or T? – reasonably well, similar to the HST broad-band filters.

progression from early to late (M0 to T8) along these two colors (Fig. 6). This strongly illustrates the need for a medium-band filter to subtype brown dwarfs and the power of a well-placed medium-band filter to do so.

Figure 6 shows the same plot but for only the SPLAT standard stars (i.e., those that define the type) from Burgasser et al. (2006), Kirkpatrick et al. (2010), and Cushing et al. (2011). This figure demonstrates how the separation in color space allows subtyping without significant degeneracy.

The broad *Euclid* filter set identifies a clear window in color–color space to identify broad types of these objects. The three near-infrared *Euclid* filter bands discriminate as well as the HST filters between broad type (Fig. 7). The near all-sky coverage of this mission will therefore result in an ideal parent sample to explore the Milky Way structure; dwarf stars will be relatively easily identified in their class of objects. However, to identify in detail what subtype of dwarf star each object is, it will require follow-up observations such as *Euclid* grism subtype identification or a proper motion measurement between *Euclid* observation epochs to determine distance and hence likely subtype.

Like *Euclid*, WFIRST/WFI is a wide-area survey instrument, designed to observe many high-latitude fields. Unlike *Euclid*, there are more filters available to discriminate among brown dwarf types. They do so with intermediate success, similar to the broad HST filters used so far. There are weak trends with broad dwarf type in many filter combinations (see Table A.3 and Fig. 8). Most of the brown dwarfs are tightly grouped in color–color space (i.e., a narrow range of values in W146-H158, see Fig. 8) with a few outliers.

The mission concepts for both *Euclid* and WFIRST are in an advanced stage, including choices for the filter combinations. It would therefore be fortuitous if a combination of WFIRST and *Euclid* filters could perform well in the subtyping of substellar dwarf. *Euclid* will cover the entire extragalactic sky and the WFIRST science case includes a very wide survey. Photometry by both mission is nearly guaranteed. However, the performance of *Euclid*/WFIRST filter combinations is a qualified success: WFIRST's W146 and F062 in combination with *Euclid*'s *Y*-band filter performs a better separation of general type than either observatory individually (see Fig. 9).

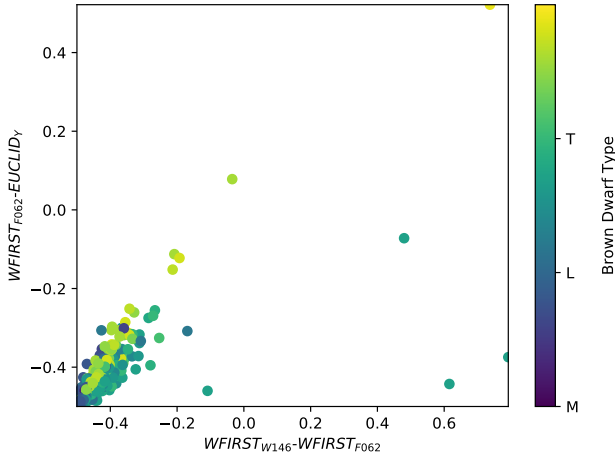**Fig. 9.** *Euclid* and WFIRST color–color plot of all the brown dwarfs in SPLAT. The W146 and F062 filters on WFIRST combined with the *Euclid Y*-band distinguish reasonably well the broad brown dwarf types with some conspicuous outliers but no better that *Euclid* alone.

Fig. 11. F814W–F105W color as a function of type for the standard red or brown dwarfs in SPLAT. Types marked similar to Fig. 10. This optical near-infrared broad filter combination comes closest to subtyping dwarf and substellar objects but is mostly not degenerate for M-dwarfs.

(e.g., Kirkpatrick et al. 2011; Pecaut & Mamajek 2013; Skrzypek et al. 2016). Similarly, Labbé et al. (2006) used Spitzer colors to reject dwarfs from their extragalactic searches. Barring deep Spitzer photometry or JWST/NIRCam observations in the 3–5 μm range, this information is not available for deep extragalactic imaging campaigns. We focus here on near-infrared filter combinations that relate linearly to type, avoiding color degeneracies.

Figure 10 shows an example of a color-type relation. To quantify the relationship between a near-infrared color and brown dwarf (sub)type, we use the Spearman ranking of the values. If there is a monotonically increasing or decreasing relationship, the Spearman ranking (ρ) is close to 1 or −1, respectively. If no such relation exists, the value is close to 0. We report Spearman rankings for the full SPLAT sample and the standard stars.

In the case of HST imaging, Holwerda et al. (2014) used the *V-J* color (F606W-F125W) to subtype the M-dwarfs once they were selected using the F098M-F125W/F125W-F160W color space. Despite some success with sub-typing, this relationship needs to be recalibrated with every new survey's filter choice targeting higher redshift objects as their choice of optical filter (to verify the dropout) continued to change. Of all the broad filters commonly used in extragalactic surveys that were evaluated, the F184W–F105W combination ($\rho = 0.98$) has the best correlation with subtype, but similar to the $V-J$ color used in Holwerda et al. (2014), the optical near-infrared color works well for M-dwarfs but becomes degenerate for later types (L+, see Fig. 11 for the relation with standard stars).

However, we now consider the medium- and narrow-band filters not commonly used in extragalactic surveys. Many combinations between a wide-band filter and one of these narrow-band filters result in a very strong correlation with red or brown dwarf spectral type. Table A.4 lists the wide/narrow-band filter combinations one could consider. The best-performing filter combination is F105W-F126N. However, the F105W filter is not always used in typical extragalactic surveys such as BoRG and CANDELS. F125W and F160W are the most commonly available. For F125W (*J*), either F127M would work almost as well as the optimal F105W-F126N combination. For F160W (*H*), the optimal narrow-band filter pairing is F153M.

To turn existing extragalactic surveys into a fast red or brown dwarf surveys of the Milky Way disk by including a single
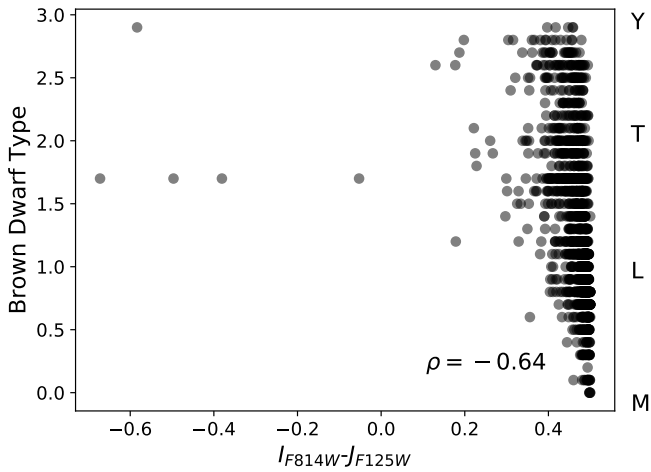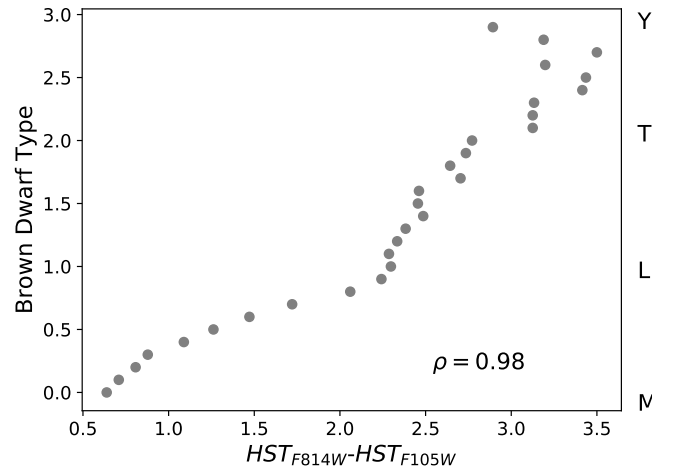

Fig. 10. HST color-type relation for brown dwarfs. red or brown dwarf types are numerical as follows: M0-M10 (0-1), L0-10 (2-3), T0-T10 (2-3) and Y0-Y3 (3-3.3). Holwerda et al. (2014) used a optical-near-infrared color (*V-J*) to subtype M-dwarfs. A optical-near-infrared color using broad filters may work well enough for M-dwarfs as type correlates with black body temperature but later types become degenerate in color space (e.g., L and T), the broad absorption features counteract the temperature effect. This makes (sub)typing difficult with only broad filters.

5. Dwarf subtyping

Brown dwarf subtyping may be achievable using a single color that has not yet been used to identify the broad type. The idea is that a combination of three (broad) filters is used to subdivide stellar objects into M/L/T-type objects and one additional filter allows for the discrimination between, for example, M3 and M5. For instance, Holwerda et al. (2014) used one separate color (*V-J*) to subtype M-type dwarfs in extragalactic fields. However, van Vledder et al. (2016) note that this kind of subtyping lets in a high level of contamination (∼50%) from other subtypes, enough to smooth out scale height differences between subtypes.

In the case of local red or brown dwarfs, the near-infrared color (e.g., the WISE W1–W2 or Spitzer [3.6]–[4.5] μm colors) can be used to probe the Rayleigh–Jeans part of the dwarf spectra and hence type them accurately photometrically
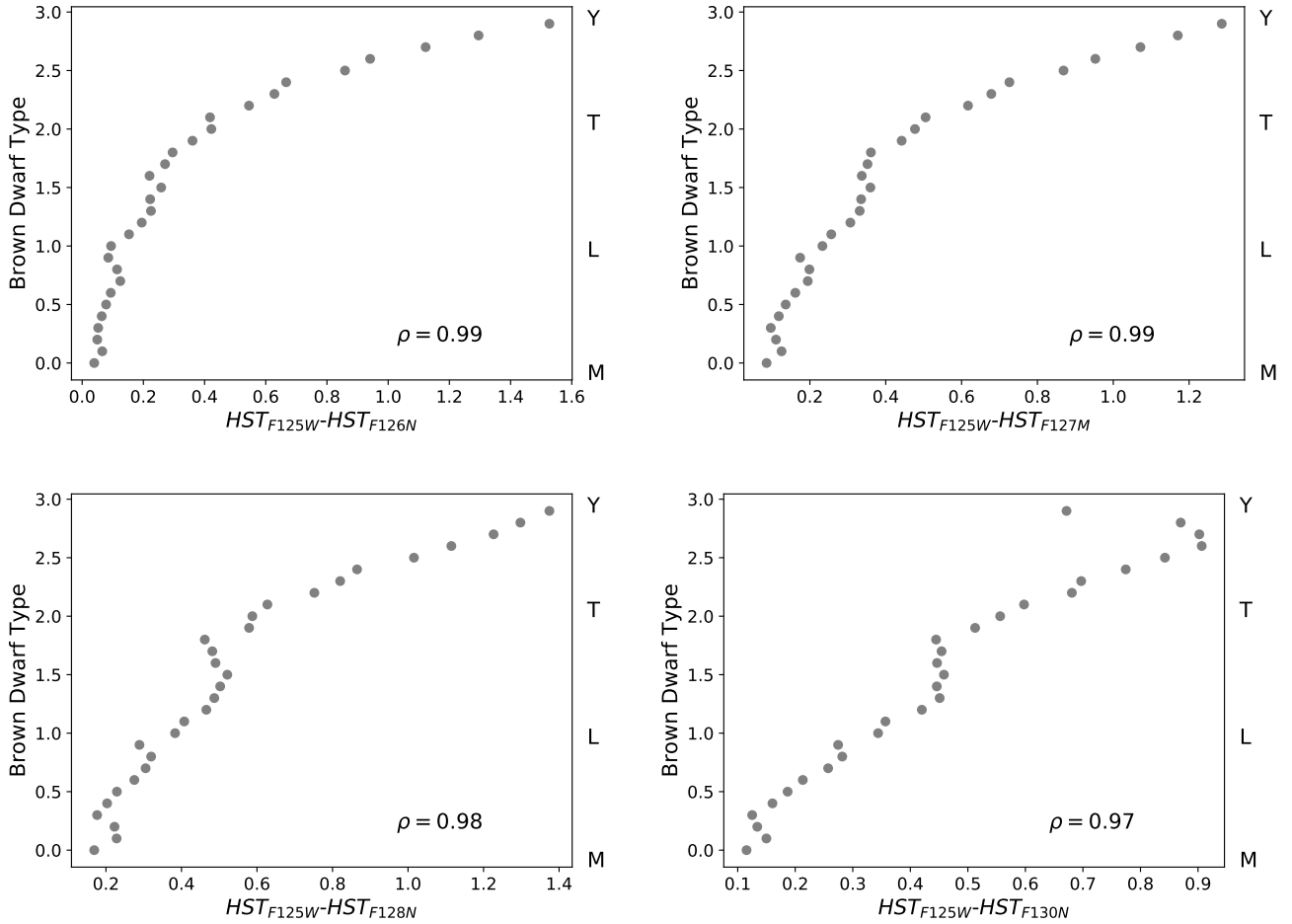
Fig. 12. Four plots showing the discriminatory power of the combination of an HST broad-band filter (F125W) with a narrow- or medium-band one for the standard stars in SPLAT: F126N (*top left panel*), F127M (*top right panel*), F128N (*bottom left panel*), and F130N (*bottom right panel*). Most extra-galactic observations feature the F125W. This is to show which medium- or narrow-band filter should be added to that to improve the (sub)typing of the brown dwarfs in these fields. All work well ($\rho > 0.90$) but the F127M stand out as an excellent compromise with a monotonous relation between the F125w-F127M color and type and highest throughput of all the considered narrow/medium bands.

medium- or narrow-band filter not previously considered, one should consider including either F126N or F127M as either one would result in excellent subtyping. Apart from the Spearman rankings, the F125W–F127M filter combination would work best with the least degeneracy in the color space (Fig. 12): each subtype has a unique color, approximately equally spaced from the neighboring types.

The next mission to consider is JWST, which a range of wide-, medium-, and narrow-band filters in this wavelength regime. Three of these stand out in their ability to separate out subtype. Figure 13 shows the brown dwarf type relation with three different color combinations using the F140M, F150W, and F162M filters onboard JWST/NIRCam. The combination of these filters differentiate the different dwarf types very well from each other. The F140M-F150W and F140M-F162M filter combisnations are equally good options to separate out red and brown dwarfs into different subtypes. The F150W-F162M combination performs slightly poorer than either of the other two filter combinations with some degeneracy in the mid L-types (Fig. 13).

We have already established that the *Euclid* filters do not separate out broad brown dwarf types well and any correlation with subtypes is nonexistent.

For WFIRST, only the Y106-F184 color ($\rho = 0.7953$) correlates best with the brown dwarf (sub)type. Both filters are close to the best-performing HST filter (*Y–I*) color. Like the HST

color-type relation in Fig. 10, it is a relation that works best for M-dwarfs but not later types.

Dwarf subtyping with combined missions

When considering combinations of HST and JWST filters, there is no filter combination that works better than one of the combinations typically already available from HST observations (see Table A.4).

While the combination of WFIRST and *Euclid* is somewhat better at identifying broad brown dwarf types (Fig. 9), the filter combination that correlates best with type, a WFIRST combination of Y106 and F184, still does not discriminate among types very well (Fig. 9 and Table A.3). WFIRST's mission concept is, at present, not an ideal follow-up instrument of brown dwarfs identified with imaging. WFIRST would be markedly better at discerning between brown dwarf types with the addition of a single medium-band filter to WFIRST's filter selection. When a medium-band filter is combined with the wide W146 filter, for example, WFIRST would become an effective mission for subtyping brown dwarfs. Arguably, this could also be done with WFIRST grism capability if done to a similar limiting depth as the imaging surveys. The typing of substellar dwarfs is one of several reasons to add a medium-wide filter but brown dwarf characterization would be the argument for one centered on the key absorption features.
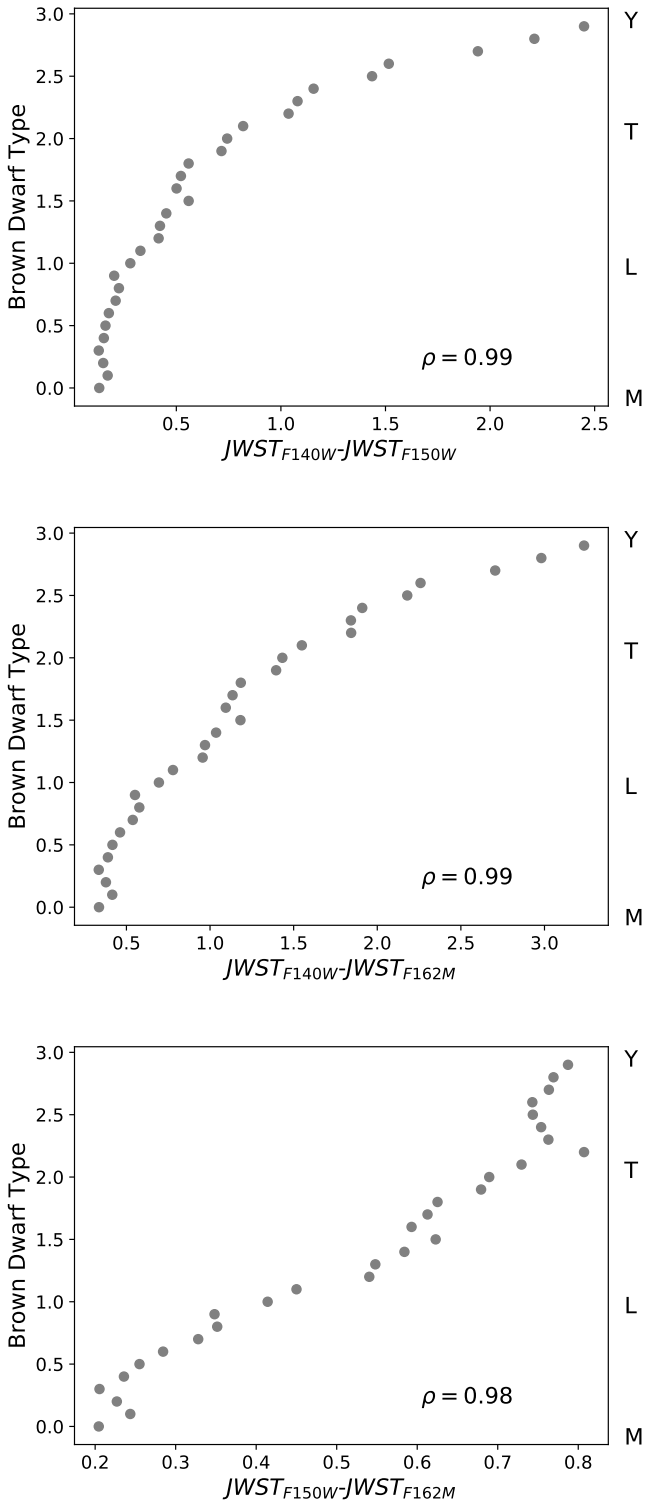
Fig. 13. Relation between three JWST colors using the optimal filter combinations and the brown dwarf type and subtype for the standard stars in SPLAT. The F140W/F150W or the F140W/F162M filter combinations result unambiguous subtyping. The F150W/F162M combinations is degenerate in the Y-dwarf category.

6. Discussion

In this work, we explore how well the current HST filter set that is typically used in high-redshift observations (e.g., CANDELS, BoRG, XDF) could discriminate between both broad and subtypes of brown dwarfs. Our second goal is to explore to what extent future near-infrared imaging observatories can be used to type and subtype brown dwarfs.

Our results show that the current filter combinations for BoRG[z8] and BoRG[z9] observations are nearly as ideal for the discrimination between broad type as is practical with the HST filters that are most commonly used for extragalactic work[3]. The ability of the BoRG[z8] and BoRG[z9] filter combinations to distinguish broad substellar type. This holds promise to use the new BoRG[z9] observations to map the Milky Way population using the many separate sightlines.

However, when all the medium- and narrow-band filters available in WFC3 are considered, good subtype separation can be achieved with the addition of just one narrow (e.g., F126N) or medium (F127M) filter to the already available F125W imaging. We note this is true for the standard stars and that the relation between color and subtype is much noisier for the whole sample in SPLAT. This offers the opportunity to supplement the extragalactic fields with just single filter observations to accurately subtype the red and brown dwarfs in these fields. For the legacy fields with grism information, this is less useful, but for the pure-parallel surveys (e.g., BoRG) this is a viable path to discriminate between subtypes and thus test the possible relation between brown dwarf cooling and the scale height of their distribution in the Milky Way (see Ryan et al. 2017).

JWST will be the most suitable upcoming mission for distinguishing brown dwarf types in terms of discretionary power, not just between broad types but with the clear potential to map colors to subtypes with reasonable accuracy.

We note that the high-redshift imaging surveys with JWST will not automatically be able to identify dwarfs, but the filter combinations that would make this possible are now known and could potentially be included in such surveys (e.g., as part of pre-imaging to avoid targeting brown dwarfs for follow-up spectroscopy for example).

Euclid will be extremely useful in mapping the broad dwarf types of the Milky Way as a whole, but subtyping, these stellar objects will be challenging without spectroscopy (e.g., grism observations) or ancillary data (ground-based optical observations of M-dwarfs, for example).

WFIRST performs better at discriminating broad dwarf types, but lacks a medium- or narrow-band filter that would be capable of discriminating among subtypes. We therefore argue strongly in favor of adding a medium-band filter in the *H*-band to the WFIRST filter wheel. While dwarf star and substellar programs alone may not constitute a strong enough science case to justify a medium-band filter, Solar System science has also expressed an interest in adding a *Ks* broad-band filter (Holler et al. 2018). Additionally, the addition of such a filter would strengthen the selection of high-redshift candidates (of order 10k objects at a given redshift) by weeding out the M/L/T dwarfs (an order or so more objects, depending on depth and target redshift). If a medium-band filter in the broad *H*-band range is considered a valuable addition to, for example, planetary science and other WFIRST mission objectives, the project should seriously consider adding one to the filter wheel.

Combining the ubiquitous *Euclid* observations (all-sky) with WFIRST observations improves the identifications of broad brown dwarf categories (M/L/T), but does not succeed at subtyping. With a need to map the initial mass function of stars galaxy-wide (El-Badry et al. 2017), a medium-band filter on WFIRST would fill the gap of knowledge between any JWST

---

[3] BoRG has a single optical filter, either F606W (broad *V*) or F350LP, which do not help with broad dwarf typing but may be of use for subtyping M-dwarfs.

observations sampling the stellar content of nearby galaxies and WFIRST observations constraining their full stellar population.

7. Concluding remarks

We group our conclusions by the narrow-field (HST and JWST) and the wide-field (*Euclid* and WFIRST) observatories:

– The HST filters used thus far for high-redshift searches (e.g., CANDELS and BoRG) are close to optimal to identify broad red or brown dwarf type (Fig. 3 and Table A.3).
– With the addition of medium- and narrow-band filters not commonly used for extragalactic surveys, a good separation of subtypes can be achieved using the F127M and F125W filters that are most commonly used for extragalactic surveys (Fig. 4 and Table A.4).
– The combination of three JWST filters (F140M, F150W, and F162M) split both the broad and subtypes of brown dwarfs (Fig. 5).
– JWST F140M and F150W is the optimal combination of filters to subtype brown dwarfs (Fig. 13). Alternatively, the combination of F150W and F162M works almost as well (Fig. 13 and Table A.4).
– *Euclid* alone performs similarly well as extragalactic HST surveys in discriminating among broad M-, L-, and T-type brown dwarfs (Fig. 7), with follow-up needed to identify subtype.
– The WFIRST filters perform similarly as HST and *Euclid*, with the optimal combination W146, H158, F062 separating broad brown dwarf types but not able to discriminate between subtypes (Fig. 8).
– The combination of *Euclid* and WFIRST, using WFIRST's W146 and F062 filters and *Euclid*'s *Y*-band filter, allows for a much better discrimination between broad brown dwarf categories (Fig. 9).
– Subsequent subtyping with the combination of *Euclid* and WFIRST observations remains uncertain due to the lack of medium- or narrow-band filters in this wavelength range (Fig. 9).

References

Ahmic, M., Jayawardhana, R., Brandeker, A., et al. 2007, ApJ, 671, 2074
Allers, K. N., Jaffe, D. T., Luhman, K. L., et al. 2007, ApJ, 657, 511
Andersen, M., Meyer, M. R., Oppenheimer, B., Dougados, C., & Carpenter, J. 2006, AJ, 132, 2296
Astropy Collaboration (Robitaille, T. P., et al.) 2013, A&A, 558, A33
Bardalez Gagliuffi, D. C., Gagné, J., Faherty, J. K., & Burgasser, A. J. 2018, ApJ, 854, 101
Beckwith, S. V. W., Stiavelli, M., Koekemoer, A. M., et al. 2006, AJ, 132, 1729
Bernard, S. R., Carrasco, D., Trenti, M., et al. 2016, ApJ, 827, 76

Brammer, G. B., van Dokkum, P. G., Franx, M., et al. 2012, ApJS, 200, 13
Burgasser, A. J. 2007, ApJ, 658, 617
Burgasser, A. J., & McElwain, M. W. 2006, AJ, 131, 1007
Burgasser, A. J., & SPLAT Development Team 2017, ASI Conf. Ser., 14, 7
Burgasser, A. J., Burrows, A., & Kirkpatrick, J. D. 2006, ApJ, 639, 1095
Burgasser, A. J., Blake, C. H., Gelino, C. R., Sahlmann, J., & Bardalez Gagliuffi D. 2016, ApJ, 827, 25
Burgasser, A. J., Theissen, C. A., Bardalez Gagliuffi, D. C., & Schlawin, E. 2017, Res. Notes Am. Astron. Soc., 1, 47
Caballero, J. A., Burgasser, A. J., & Klement, R. 2008, A&A, 488, 181
Calvi, V., Trenti, M., Stiavelli, M., et al. 2016, ApJ, 817, 120
Cruz, K. L., Reid, I. N., Kirkpatrick, J. D., et al. 2007, AJ, 133, 439
Cushing, M. C., Kirkpatrick, J. D., Gelino, C. R., et al. 2011, ApJ, 743, 50
Da Rio, N., Robberto, M., Hillenbrand, L. A., Henning, T., & Stassun, K. G. 2012, ApJ, 748, 14
Dieterich, S. B., Henry, T. J., Jao, W.-C., et al. 2014, AJ, 147, 94
Dressler, A., Spergel, D., Mountain, M., et al. 2012, ArXiv e-prints [arXiv:1210.7809]
Dupuy, T. J., & Liu, M. C. 2012, ApJS, 201, 19
El-Badry, K., Weisz, D. R., & Quataert, E. 2017, MNRAS, 468, 319
Giavalisco, M., Ferguson, H. C., Koekemoer, A. M., et al. 2004, ApJ, 600, L93
Grogin, N. A., Kocevski, D. D., Faber, S. M., et al. 2011, ApJS, 197, 35
Holler, B. J., Milam, S. N., Bauer, J. M., et al. 2018, J. Astron. Telesc. Inst. Syst., 4, 034003
Holwerda, B. W., Trenti, M., Clarkson, W., et al. 2014, ApJ, 788, 77
Hunter, J. D. 2007, Comput. Sci. Eng., 9, 90
Joergens, V., Neuhäuser, R., Guenther, E. W., Fernández, M., & Comerón, F. 2003, IAU Symp., 211, 233
Jones, E., Oliphant, T., Peterson, P., & Others. 2001, SciPy: Open source scientific tools for Python
Kimble, R. A., MacKenty, J. W., O'Connell, R. W., & Townsend, J. A. 2008, Proc. SPIE, 7010, 70101E
Kirkpatrick, J. D. 2005, ARA&A, 43, 195
Kirkpatrick, J. D., Looper, D. L., Burgasser, A. J., et al. 2010, ApJS, 190, 100
Kirkpatrick, J. D., Cushing, M. C., Gelino, C. R., et al. 2011, ApJS, 197, 19
Kirkpatrick, A., Calzetti, D., Kennicutt, R., et al. 2014, ApJ, 789, 130
Kirkpatrick, J. D., Kellogg, K., Schneider, A. C., et al. 2016, ApJS, 224, 36
Koekemoer, A. M., Faber, S. M., Ferguson, H. C., et al. 2011, ApJS, 197, 36
Kuchner, M. J., Faherty, J. K., Schneider, A. C., et al. 2017, ApJ, 841, L19
Labbé, I., Bouwens, R., Illingworth, G. D., & Franx, M. 2006, ApJ, 649, L67
Laureijs, R., Amiaux, J., Arduini, S., et al. 2011, ArXiv e-prints [arXiv:1110.3193]
Masters, D., McCarthy, P., Burgasser, A. J., et al. 2012, ApJ, 752, L14
Momcheva, I. G., Brammer, G. B., van Dokkum, P. G., et al. 2016, ApJS, 225, 27
Najita, J. R., Tiede, G. P., & Carr, J. S. 2000, ApJ, 541, 977
Opitz, D., Tinney, C. G., Faherty, J. K., et al. 2016, ApJ, 819, 17
Pecaut, M. J., & Mamajek, E. E. 2013, ApJS, 208, 9
Pirzkal, N., Sahu, K. C., Burgasser, A., et al. 2005, ApJ, 622, 319
Pirzkal, N., Burgasser, A. J., Malhotra, S., et al. 2009, ApJ, 695, 1591
Pirzkal, N., Malhotra, S., Ryan, R. E., et al. 2017, ApJ, 846, 84
Reid, I. N., Burgasser, A. J., Cruz, K. L., Kirkpatrick, J. D., & Gizis, J. E. 2001, AJ, 121, 1710
Robert, J., Gagné, J., Artigau, É., et al. 2016, ApJ, 830, 144
Ryan, Jr., R. E., Hathi, N. P., Cohen, S. H., & Windhorst, R. A. 2005, ApJ, 631, L159
Ryan, R. E., Thorman, P. A., Yan, H., et al. 2011, ApJ, 739, 83
Ryan, Jr., R. E., Thorman, P. A., Schmidt, S. J., et al. 2017, ApJ, 847, 53
Shan, Y., Yee, J. C., Bowler, B. P., et al. 2017, ApJ, 846, 93
Skelton, R. E., Whitaker, K. E., Momcheva, I. G., et al. 2014, ApJS, 214, 24
Skrzypek, N., Warren, S. J., & Faherty, J. K. 2016, A&A, 589, A49
Spergel, D., Gehrels, N., Breckinridge, J., et al. 2013, ArXiv e-prints [arXiv:1305.5425]
Spergel, D., Gehrels, N., Baltay, C., et al. 2015, ArXiv e-prints [arXiv:1503.03757]
Straughn, A. N., Pirzkal, N., Meurer, G. R., et al. 2009, AJ, 138, 1022
Testi, L., D'Antona, F., Ghinassi, F., et al. 2001, ApJ, 552, L147
Theissen, C. A., Burgasser, A. J., Bardalez Gagliuffi, D. C., et al. 2018, ApJ, 853, 75
Thompson, R., Green, J., Rieke, G., et al. 2013, ArXiv e-prints [arXiv:1312.4548]
Tilvi, V., Pirzkal, N., Malhotra, S., et al. 2016, ApJ, 827, L14
Tinney, C. G., Faherty, J. K., Kirkpatrick, J. D., et al. 2012, ApJ, 759, 60
Tinney, C. G., Faherty, J. K., Kirkpatrick, J. D., et al. 2014, ApJ, 796, 39
Trenti, M., Bradley, L. D., Stiavelli, M., et al. 2011, ApJ, 727, L39
van Vledder, I., van der Vlugt, D., Holwerda, B. W., et al. 2016, MNRAS, 458, 425
Ward-Duong, K., Patience, J., De Rosa, R. J., et al. 2015, MNRAS, 449, 2618
Wilkins, S. M., Stanway, E. R., & Bremer, M. N. 2014, MNRAS, 439, 1038

Appendix A: Tables

Table A.1. Apparent magnitudes of all SPLAT sources computed in the HST filters.

Number	index type	unc	st. type	unc	f814w	err	f098m	err	f105w	err	f125w	err	f140w	err	f160w	err
10209	2.45	0.251874	2.4	0.5	29.372312	0.737955	26.388198	0.019829	26.040271	0.017670	25.151282	0.010545	24.976077	0.014932	25.012600	0.018229
11855	1.10	0.556161	0.9	0.5	26.141540	0.047187	24.378857	0.008233	23.993578	0.005929	23.258797	0.005871	23.019959	0.005195	22.749328	0.004908
11044	1.50	1.446706	0.7	0.5	-11.486000	0.116757	-12.871494	0.021930	-13.122074	0.017582	-13.691276	0.014701	-13.881244	0.015448	-14.066726	0.019746
11982	1.45	0.782517	0.8	0.5	28.966369	0.249016	27.058639	0.027124	26.666028	0.023796	25.942172	0.017572	25.812199	0.028278	25.618098	0.027475
11421	1.70	1.172794	1.5	0.5	28.005479	1.083947	26.099946	0.162242	25.620674	0.092142	24.727244	0.060927	24.404745	0.053707	23.995905	0.066472
11247	1.55	0.550069	1.5	0.5	26.594247	0.063245	24.575206	0.007908	24.030100	0.006780	23.055668	0.008470	22.736875	0.007388	22.343638	0.004645
11698	1.15	0.771520	0.8	0.5	-10.935690	0.031929	-12.632574	0.005225	-12.965344	0.004880	-13.609522	0.004166	-13.786967	0.004354	-13.995748	0.004867
11141	1.40	0.605644	1.2	0.5	-10.322486	0.198560	-12.062434	0.029495	-12.590032	0.017821	-13.522434	0.009380	-13.818142	0.014007	-14.169966	0.012898
...	...	...	...	...	...	...	...	...	...	...	...	...	...	...	...	...

Number	f110w	err	f126n	err	f127m	err	f128n	err	f130n	err	f132n	err	f139m	err	f153m	err	f164n	err	f167n	err
10209	25.586065	0.014592	24.407990	0.001543	24.377040	0.004786	24.231875	0.005564	24.371324	0.006726	24.599358	0.007122	26.993115	0.017207	24.726078	0.016803	24.574274			
11855	23.686045	0.006147	23.148405	0.001903	23.050387	0.003815	22.917331	0.003717	22.957785	0.004465	22.910851	0.004144	23.128230	0.004539	22.732345	0.005327	22.361824			
11044	-13.352015	0.018002	-13.769097	0.009927	-13.833643	0.007117	-13.917844	0.011190	-13.931957	0.018427	-13.933358	0.008718	-13.858432	0.015810	-14.064632	0.019727	-14.364993			
11982	26.363584	0.019801	25.731165	0.002699	25.606229	0.013378	25.456794	0.013156	25.504963	0.017095	25.515775	0.014354	26.200514	0.013234	25.630973	0.036443	25.036492			
11421	25.219328	0.080270	24.521394	0.003457	24.399724	0.030904	24.249587	0.048754	24.282875	0.061165	24.251556	0.028959	24.735634	0.086233	23.945005	0.060995	23.451594			
11247	23.582249	0.008403	22.880789	0.024412	22.722187	0.003389	22.548876	0.002531	22.595052	0.001526	22.532386	0.003459	23.103446	0.003934	22.293263	0.003764	21.810253			
11698	-13.225395	0.004635	-13.723168	0.011128	-13.826193	0.003293	-13.961135	0.003169	-13.912346	0.003625	-13.938581	0.002976	-13.614185	0.003013	-14.004456	0.004954	-14.386689			
11141	-13.008769	0.014654	-13.682035	0.011464	-13.819253	0.008707	-13.992386	0.009125	-13.944113	0.010182	-14.000426	0.008279	-13.592730	0.007713	-14.199573	0.011799	-14.658427			
...	...	...	...	...															

Notes. Full tables for all four missions considered available at the CDS with this publication.

Table A.2. Apparent magnitudes of the standard stars in SPLAT computed in the HST filters.

type	f814w	err	f098m	err	f105w	err	f125w	err	f140w	err	f160w	err
0.000000	15.899930	0.001543	15.391747	0.001118	15.261395	0.001002	14.869515	0.000965	14.626093	0.000908	14.375303	0.001027
0.100000	14.854688	0.001903	14.280802	0.001044	14.145593	0.000972	13.773502	0.000825	13.553462	0.000915	13.308419	0.001013
0.200000	15.702178	0.009927	15.042564	0.006830	14.894865	0.006286	14.479290	0.006014	14.231508	0.004051	13.974077	0.001843
0.300000	14.611093	0.002699	13.882720	0.001286	13.732808	0.001237	13.326169	0.001144	13.107942	0.000999	12.882308	0.000879
0.400000	16.368592	0.003457	15.462166	0.001011	15.279736	0.000793	14.813992	0.000642	14.581105	0.000616	14.341436	0.000561
0.500000	17.839593	0.024412	16.780626	0.006790	16.577970	0.005355	16.090950	0.003326	15.881036	0.003220	15.662715	0.002252
0.600000	18.462491	0.011128	17.226143	0.006864	16.990912	0.007171	16.465313	0.005783	16.263692	0.004715	16.046787	0.002890
0.700000	19.690574	0.011464	18.236665	0.002748	17.969519	0.002390	17.415236	0.002319	17.245658	0.002314	17.053054	0.001763
0.800000	20.130288	0.017328	18.405429	0.003826	18.070077	0.003053	17.412810	0.003053	17.215094	0.002582	16.994888	0.002360
0.900000	22.103708	0.023542	20.268131	0.005144	19.861593	0.004005	19.096285	0.004005	18.877246	0.003753	18.646106	0.003500
1.000000	24.744026	0.099897	22.886584	0.018988	22.446538	0.018206	21.652739	0.018206	21.416498	0.013475	21.144286	0.013363
1.100000	-10.494208	0.056565	-12.332495	0.010081	-12.780326	0.006745	-13.579649	0.006745	-13.817763	0.004967	-14.101498	0.004503
1.200000	-10.289958	0.091685	-12.118031	0.013882	-12.624098	0.009503	-13.523631	0.009503	-13.801444	0.007654	-14.147596	0.006884
1.300000	-10.177335	0.186718	-12.037084	0.022890	-12.560805	0.017159	-13.494929	0.017159	-13.774356	0.012136	-14.116088	0.011859
1.400000	26.296216	0.228449	24.328822	0.033099	23.810042	0.022603	22.881367	0.022603	22.623482	0.016774	22.287825	0.019745
1.500000	27.106031	0.878145	25.151953	0.106404	24.650891	0.082973	23.728704	0.082973	23.415076	0.036829	23.008029	0.039664
1.600000	29.001420	0.241383	27.025268	0.031174	26.540100	0.031174	25.594836	0.021834	25.255701	0.014802	24.844285	0.011932

type	f110w	err	f126n	err
0.000000	15.105016	0.000860	14.830084	0.000818
0.100000	14.000394	0.000991	13.707886	0.000826
0.200000	14.729068	0.005834	14.429890	0.004371
0.300000	13.573269	0.000882	13.273774	0.000862
0.400000	15.094559	0.000832	14.750009	0.000475
0.500000	16.384756	0.004814	16.012595	0.002400
0.600000	16.782723	0.007193	16.371868	0.004267
0.700000	17.751195	0.002383	17.290638	0.001944
0.800000	17.802972	0.002592	17.298781	0.001991
0.900000	19.539159	0.003206	19.010867	0.002669
1.000000	22.111148	0.017162	21.558256	0.013655
1.100000	-13.119392	0.005727	-13.732771	0.003828
1.200000	-13.024292	0.007977	-13.718354	0.004889
1.300000	-12.983060	0.011522	-13.719778	0.006404
1.400000	23.391235	0.021655	22.659144	0.009118
1.500000	24.231876	0.050880	23.470363	0.029227
1.600000	26.103488	0.017385	25.374709	0.011522

Notes. Full tables for all four missions considered available at the CDS with this publication.

Table A.2. continued.

type	f127m	err	f128n	err	f130n	err	f132n	err	f139m	err	f153m	err	f164n	err	f167n	err
1.700000	27.507458	0.451258	25.263335	0.040385	24.803500	0.026976	23.846489	0.017546	23.471683	0.018497	23.024781	0.017005	24.350617	0.021934	23.575645	0.012359
1.800000	27.110130	0.613350	24.879452	0.036599	24.466824	0.028260	23.554237	0.027429	23.177565	0.031327	22.718103	0.028558	24.037548	0.029152	23.258687	0.023045
1.900000	26.508975	0.354354	24.183902	0.025975	23.773832	0.015019	22.904929	0.024973	22.547602	0.022890	22.088120	0.013392	23.373041	0.022646	22.544341	0.009017
2.000000	27.009912	0.265701	24.632475	0.023881	24.238698	0.018373	23.391026	0.012787	23.114955	0.012633	22.762825	0.011700	23.845894	0.012924	22.968935	0.007790
2.100000	28.690396	0.923623	25.936288	0.069293	25.565081	0.045821	24.746977	0.029511	24.504619	0.035155	24.183535	0.035088	25.184462	0.036782	24.329196	0.019452
2.200000	-9.207141	0.346215	-11.947037	0.027084	-12.332387	0.022844	-13.215783	0.019505	-13.455624	0.017961	-13.756934	0.024540	-12.762294	0.020081	-13.761028	0.007704
2.300000	30.155773	1.000065	27.364090	0.040006	27.022633	0.032188	26.199667	0.026212	25.980341	0.025047	25.806879	0.028144	26.618906	0.026953	25.571468	0.012710
2.400000	-8.694234	0.420600	-11.698319	0.024193	-12.109211	0.018304	-13.059519	0.010441	-13.255685	0.015690	-13.300924	0.018336	-12.591110	0.015084	-13.726048	0.004460
2.500000	-8.549112	0.347421	-11.678520	0.018601	-11.985034	0.014403	-12.901239	0.011585	-13.072898	0.014591	-12.844708	0.024555	-12.476895	0.012099	-13.760193	0.006258
2.600000	29.991384	0.773039	27.071246	0.029344	26.793195	0.024424	25.799084	0.019202	25.595478	0.023286	25.905353	0.031616	26.229258	0.022278	24.858067	0.006808
2.700000	30.448999	1.103697	27.126489	0.044075	26.949189	0.036304	25.966605	0.020832	25.704727	0.030168	26.075032	0.051842	26.361753	0.028608	24.844237	0.011778
2.800000	29.948017	0.783433	26.908346	0.023648	26.759056	0.022226	25.703298	0.015412	25.350569	0.016513	25.629902	0.029105	26.103868	0.016178	24.407874	0.005125
2.900000	30.917000	0.881172	28.052596	0.042853	28.024125	0.045980	27.142792	0.036705	26.725816	0.037469	27.013187	0.066687	27.445632	0.031774	25.615928	0.009531
0.000000	14.783623	0.000793	14.700590	0.000830	14.754157	0.000894	14.733106	0.000851	14.586792	0.001423	14.369414	0.000989	14.163077	0.000947	14.194602	0.001113
0.100000	13.648148	0.000755	13.545283	0.000861	13.623641	0.000800	13.608124	0.000885	13.631821	0.001444	13.292160	0.000886	13.078941	0.000978	13.102232	0.000981
0.200000	14.368598	0.004710	14.256646	0.004087	14.345302	0.003254	14.318873	0.003554	14.236413	0.010730	13.966399	0.001287	13.752624	0.000890	13.777591	0.001064
0.300000	13.229219	0.000912	13.149576	0.000855	13.201040	0.000657	13.179915	0.000841	13.094307	0.001748	12.878076	0.000817	12.674388	0.000873	12.693066	0.000739
0.400000	14.695918	0.000561	14.610911	0.000505	14.653582	0.000494	14.625309	0.000513	14.595311	0.001239	14.331436	0.000522	14.110528	0.000545	14.118771	0.000549
0.500000	15.954698	0.002661	15.861983	0.002482	15.904212	0.002485	15.875232	0.002724	15.922700	0.004876	15.652497	0.002480	15.406575	0.002257	15.401854	0.002174
0.600000	16.303667	0.004446	16.190199	0.005202	16.252163	0.003926	16.230800	0.003304	16.318688	0.008149	16.047508	0.002219	15.756212	0.002933	15.759329	0.003291
0.700000	17.220826	0.001506	17.110254	0.001818	17.158068	0.001576	17.143415	0.001623	17.365278	0.003808	17.046260	0.002109	16.720733	0.001564	16.702244	0.001713
0.800000	17.214076	0.001981	17.093139	0.001820	17.131105	0.001721	17.098945	0.001781	17.333887	0.005295	16.983724	0.002007	16.639809	0.001650	16.621532	0.001750
0.900000	18.921996	0.002929	18.807569	0.002711	18.821771	0.002674	18.764090	0.002541	18.894676	0.016629	18.644729	0.003201	18.279693	0.003100	18.255598	0.003109
1.000000	21.419669	0.014155	21.269720	0.013574	21.308717	0.013770	21.271402	0.007237	21.581955	0.006016	21.131820	0.010241	20.752074	0.010630	20.724678	0.009306
1.100000	-13.836052	0.003597	-13.986955	0.004018	-13.936387	0.003849	-13.984065	0.003181	-13.607015	0.015841	-14.141812	0.004562	-14.533039	0.003968	-14.549914	0.004152
1.200000	-13.830464	0.005378	-13.989410	0.004960	-13.943684	0.004197	-13.998707	0.004810	-13.524781	0.016063	-14.173500	0.005629	-14.667099	0.004756	-14.691105	0.004243
1.300000	-13.826311	0.008380	-13.981797	0.007555	-13.945934	0.006973	-13.972631	0.008361	-13.513218	0.055254	-14.133375	0.013291	-14.642582	0.008693	-14.681513	0.009229
1.400000	22.546164	0.010798	22.378866	0.012281	22.435334	0.010497	22.389697	0.010421	22.903040	0.062297	22.272367	0.017188	21.725578	0.011805	21.689883	0.013453
1.500000	23.369098	0.029498	23.207328	0.034722	23.270314	0.026719	23.213718	0.038970	23.839673	0.020240	22.951460	0.036749	22.433557	0.034081	22.428289	0.033647
1.600000	25.257928	0.015131	25.104765	0.018181	25.148398	0.012580	25.078741	0.009620	25.587854	0.034608	24.804208	0.010279	24.302830	0.007837	24.269766	0.008438
1.700000	23.494574	0.013865	23.364886	0.015160	23.392163	0.012365	23.350688	0.011127	23.762839	0.059749	23.006614	0.014468	22.458487	0.010767	22.430675	0.010420
1.800000	23.193358	0.019714	23.092559	0.023687	23.109466	0.025067	23.087771	0.018796	23.504790	0.154212	22.690472	0.029055	22.142752	0.022424	22.122829	0.021579
1.900000	22.462936	0.007256	22.325836	0.009688	22.392331	0.005775	22.424173	0.011394	23.154931	0.049167	22.007046	0.011298	21.490820	0.004501	21.502957	0.006692
2.000000	22.913919	0.007579	22.803333	0.007163	22.834888	0.007287	22.864492	0.007241	23.865499	0.123533	22.660831	0.011524	22.164018	0.007926	22.189194	0.008374
2.100000	24.241748	0.018745	24.119494	0.019296	24.149339	0.018603	24.172130	0.017187	25.370212	0.074376	24.105119	0.037800	23.528799	0.022701	23.548109	0.023805
2.200000	-13.832774	0.011954	-13.967727	0.014547	-13.896515	0.014923	-13.811501	0.011333	-12.208080	0.150409	-13.846490	0.022130	-14.435888	0.010848	-14.396686	0.020042
2.300000	25.521290	0.014615	25.379409	0.015490	25.502703	0.012380	25.636102	0.013254	27.551760	0.093878	25.614419	0.025308	25.285149	0.021292	25.324547	0.025732
2.400000	-13.785658	0.005676	-13.924480	0.007166	-13.833914	0.009277	-13.696647	0.009550	-11.545001	0.120726	-13.547346	0.013853	-13.733687	0.013750	-13.635231	0.023131
2.500000	-13.770058	0.004990	-13.916881	0.005098	-13.743727	0.002974	-13.439327	0.018078	-10.445431	0.738226	-13.241676	0.017079	-13.071657	0.015150	-12.849973	0.032326
2.600000	24.846328	0.010674	24.684421	0.011652	24.892664	0.012939	25.205128	0.010705	28.434166	0.724467	25.471823	0.020860	25.876853	0.023218	26.028462	0.031771
2.700000	24.894955	0.009334	24.740085	0.007872	25.064345	0.009808	25.570628	0.011345	29.324037	0.976734	25.554014	0.031693	26.395775	0.077805	26.622422	0.098748
2.800000	24.533197	0.005388	24.405737	0.005818	24.833399	0.007985	25.443075	0.011160	30.124869	1.400790	25.094454	0.017494	26.414867	0.063849	26.627387	0.082270
2.900000	25.856703	0.011106	25.768459	0.012957	26.471303	0.018044	27.345420	0.034229	30.682969		26.474543	0.038656	28.286133	0.251635	28.909125	0.589481

Table A.3. Top three Spearman rankings between type and subtype and two-colors using filter combinations onboard HST, JWST, and WFIRST, using the standard stars in SPLAT.

Filter combination	Spearman ranking (ρ) and validity (p-value)
HST	
$I_{F814W}-Y_{F098M}$ & $Y_{F098M}-JH_{F140W}$	0.8186 (0.00)
$I_{F814W}-Y_{F105W}$ & $Y_{F105W}-JH_{F140W}$	0.8179 (0.00)
$I_{F814W}-J_{F125W}$ & $J_{F125W}-JH_{F140W}$	**0.8197** (0.00)
JWST	
$F070W-F115W$ & $F115W-F150W$	0.8215 (0.00)
$F070W-F115W$ & $F115W-F162M$	0.8581 (0.00)
$F140M-F150W$ & $F150W-F162M$	**0.9897** (0.00)
WFIRST	
$W146-F062$ & $F062-H158$	0.6807 (0.00)
$W146-H158$ & $H158-F062$	**0.6922** (0.00)
$J129-H158$ & $H158-F062$	0.6624 (0.00)

Table A.4. Top three Spearman rankings between (sub)type and a single filter combination onboard HST, JWST, or WFIRST, and the HST/JWST and *Euclid*/WFIRST combinations using all the stars in SPLAT.

Filter combination	Spearman ranking (ρ)
HST (broad filters)	
$Y_{F098M}-J_{F125W}$	0.7686 (0.00)
$Y_{F098M}-JH_{F140W}$	0.7738 (0.00)
$Y_{F098M}-H_{F160W}$	**0.7769** (0.00)
HST (broad/medium/narrow filters)	
$Y_{F098M}-H_{F160W}$	0.7784 (0.00)
$Y_{F098M}-F110W$	0.7791 (0.00)
$Y_{F098M}-F164N$	**0.7817** (0.00)
HST (F125W+medium/narrow filters)	
$J_{F125W}-F126N$	0.5436 (0.00)
$J_{F125W}-F127M$	0.6877 (0.00)
$J_{F125W}-F128N$	0.7226 (0.00)
$J_{F125W}-F130N$	0.7208 (0.00)
$J_{F125W}-F132N$	0.7152 (0.00)
$J_{F125W}-F139M$	0.6792 (0.00)
JWST	
$F0790W-F115W$	0.9911 (0.00)
$F140M-F150W$	0.9898 (0.00)
$F140M-F162M$	**0.9933** (0.00)
WFIRST	
$WFIRST_{Y106}-WFIRST_{J129}$	0.7879 (0.00)
$WFIRST_{Y106}-WFIRST_{H158}$	0.7761 (0.00)
$WFIRST_{Y106}-WFIRST_{f184}$	**0.7953** (0.00)
HST/JWST	
$F140M-F150W$	**0.6827** (0.00)
$F140M-F162M$	0.6761 (0.00)
$F150W-F162M$	0.6634 (0.00)
***Euclid*/WFIRST**	
$Euclid_H-WFIRST_{Y106}$	−0.7787 (0.00)
$WFIRST_{Y106}-WFIRST_{J129}$	0.7879 (0.00)
$WFIRST_{Y106}-WFIRST_{f184}$	**0.7953** (0.00)